

Automatika

Journal for Control, Measurement, Electronics, Computing and Communications



ISSN: 0005-1144 (Print) 1848-3380 (Online) Journal homepage: <https://www.tandfonline.com/loi/taut20>

Integrated fuzzy and phase shift controller for output step voltage control in multilevel inverter with reduced switch count

Jawahar Rahila & M. Santhi

To cite this article: Jawahar Rahila & M. Santhi (2020) Integrated fuzzy and phase shift controller for output step voltage control in multilevel inverter with reduced switch count, *Automatika*, 61:2, 238-249, DOI: [10.1080/00051144.2019.1680010](https://doi.org/10.1080/00051144.2019.1680010)

To link to this article: <https://doi.org/10.1080/00051144.2019.1680010>



© 2020 The Author(s). Published by Informa UK Limited, trading as Taylor & Francis Group



Published online: 04 Nov 2019.



Submit your article to this journal [↗](#)



Article views: 618



View related articles [↗](#)



View Crossmark data [↗](#)



Integrated fuzzy and phase shift controller for output step voltage control in multilevel inverter with reduced switch count

Jawahar Rahila^a and M. Santhi^b

^aSethu Institute of Technology, Pulloor, India; ^bSolamalai College of Engineering, Veerapanjan, India

ABSTRACT

A modified multilevel inverter with a configurable level generation is proposed in this paper. The MLI is composed of a modified boost converter at the front end followed by a level generation circuit and a H-bridge configuration. The front-end converter is biased with a PV source with a Hybrid boost resonant converter. The switches are triggered out of phase through a MPP tracker which uses Fractional INC MPPT. The secondary side of the circuit is composed of a derived voltage doubler along with the voltage regulator. The output of the doubler is regulated through a level converter which integrates a fuzzy controller and a phase shift controller. The modified multilevel inverter uses a low-voltage PV source as input and generates a variable-step multilevel output voltage with lower harmonic distortion and it is suitable for low-power PV applications.

ARTICLE HISTORY

Received 6 April 2019
Accepted 7 October 2019

KEYWORDS

Fuzzy logic; phase shift control; multilevel inverter; MPPT; n level

1. Introduction

PV (photovoltaic sources) is the foremost energy source after fossil fuels due to its energy generation from the environmental hazards. The PV sources have a low voltage profile that requires a converter circuit before it to match the load or grid requirements [1–5]. The PV-generated DC source is always increased by higher DC voltage and continues to give DC to DC–AC power converters. Multilevel inverters are the mostly used DC–AC converters due to their multilevel in the sine output with reduced harmonics and increased quality.

The PV source voltage has to be boosted to a required higher level to meet the appropriate load or the grid requirements. The traditional boost and buck–boost converters are the most popularly used preconditioners to boost the low-voltage input. The traditional DC–DC converters are able to operate with a voltage gain of about five times of the input voltage with a moderate efficiency at the duty cycle equal to 80%. Increasing the output voltage gain would drastically increase the duty ratio that results in the generation of greater voltage spikes associated with high conduction losses and also high reverse-recovery problems in the conducting diodes [6].

Since PV systems would require a higher static and dynamic gain around 10–20 times, it is not possible with the traditional boost converters to produce higher voltage gain. As, the traditional boost converter suffers from losses due to the presence of switches, diodes and filter elements. However, increased voltage gain is possible through extreme duty ratio. But, high peak

current is associated with output diode and it also suffers from serious reverse-recovery problems and higher current stress. This results in the poor conversion efficiency which limits power output. Hence there is a demand for a DC–DC converter with higher gain and high efficiency for a wide range of operations in power conversion.

Power conversion stages for photovoltaic applications require a compliant system which is proficient in responding to a broader range of input voltage and current variations. There have been various methods to adapt large voltage variation and high gain based on isolated and non-isolated schemes. Generally, the isolated schemes are preferred in order to reduce ground leakage current, achieve optimal voltage boost ratio and ensure safer operation when a fault occurs [7,8]. Moreover, the isolated DC–DC stage must maintain very good performance during light load conditions for a broader range of PV voltages and also have better conversion efficiency at full power [9].

A new isolated DC–DC converter with a high gain is proposed in [10]. This system constitutes a dual-switch high step-up isolated converter with voltage boost. Improvement in step-up gain in the proposed converter is achieved by employing a transformer with a lesser turns ratio. The converter suffers from the higher circulating current across the two active switches which reduce the conversion efficiency. In [11–13], a continuous-current-mode (CCM) flyback converter is suggested which benefits in simpler topology and less circulating energy. But the main switches and diodes

present in the topological circuit suffer from higher switching losses and a degraded conversion efficiency which is typically less than 90%.

In order to improve the efficiency under higher gain, including transformer leakage inductance would be an aspect. Hence utilizing the leakage current of the transformer for zero voltage switching (ZVS) of the primary switch would reduce the circulating currents across the switches which, in turn, could improve the energy efficiency [14,15]. In [16], a series resonant converter with a voltage doubler at the output end is proposed to improve the voltage gain, and in [17], an LLC-type resonant converter is incorporated for high step-up connections. In both the systems, the converter tends to operate at appropriate resonance of the LC circuit. As the PV source is vulnerable to environmental conditions, the higher voltage variations will push the converter to operate out of the divergence which results in increasing circulation energy that leads to the conversion losses.

The PV system generates power based on the solar irradiance. When the irradiance varies, the power output varies and it is mandatory to operate the system at its peak power. Hence, maximum power point trackers are implemented. These MPP trackers should obtain maximum power output efficiency of photovoltaic power systems under any climatic conditions becomes an important issue.

Generally, P&O and INC are the two major MPP trackers that are utilized due to their simplicity and the lesser computation complexity. These methods use the perturbation to track the MPP and suffer from peak oscillations at the peak point. Due to the peak oscillations, there would be some energy loss to improve the energy oscillations, a variety of MPP techniques have been discussed such as voltage feedback method, power feedback method, INC [18–21], and perturbation and observation (P&O) [22]. Non-linear behaviour of the panels, i.e. fractional-order change, would be more accurate to track peak power under larger varying conditions.

The PV systems would possess a fractional-order behaviour while the power generated by photocurrent crosses P–N junction. The relations between the diffusion current and the environmental temperature can be described as a fractional order. In order to obtain maximum power point under peak points, this paper proposes a modified incremental conductance based on the fractional-order tracking to obtain peak power transfer under power variations. These trackers operate based on the power curve profile for a fractional time to approximate the power variations which suits them for good power tracking in transient and steady-state conditions.

This topology comprises a hybrid boost resonant converter followed by a transformer and a voltage doubler. The H-bridge is used to produce a bipolar

multilevel pattern. This work resolves issues in capacitor charging, which produces exponential voltage rise of step voltage that failed to get a full step voltage within its step time. Therefore, a fuzzy and phase shift controller is used for generating full V_{step} in each step of the output. This is done by giving full D_{max} to charge the output capacitors up to 90% of V_{step} and then the control is taken by fuzzy that is phase-shifted by the secondary switches.

2. Configuration of the proposed multilevel inverter

The block diagram and the multilevel inverter converter circuit of the proposed system are shown in Figures 1(a,b). The system comprises a front-end DC–DC conversion circuit which is given as a supply for a back-end voltage regulator and a level generator. The voltage regulator is controlled to achieve sine pattern waveforms and multilevel output is generated by the level synthesizer at the back end. A fractional tracking fuzzy maximum power point tracker is implemented to extract the maximum power from the PV through duty cycle variations; furthermore, an H-bridge is incorporated to convert the unipolar wave pattern to the bipolar form.

2.1. Hybrid boost resonant converter

The front end of the converter is designed from the traditional boost converter, in which an additional switch is used to form a hybrid boost resonant converter, as

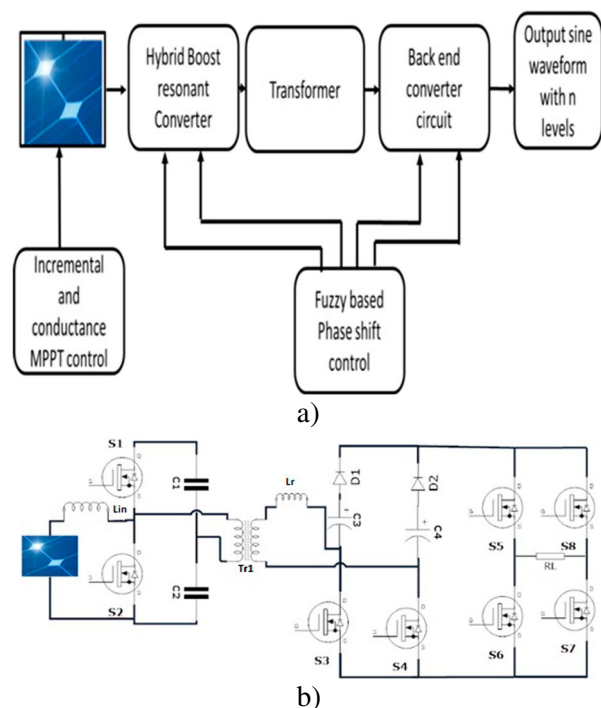


Figure 1. (a) Block diagram of the proposed system; (b) configuration of the multilevel inverter.

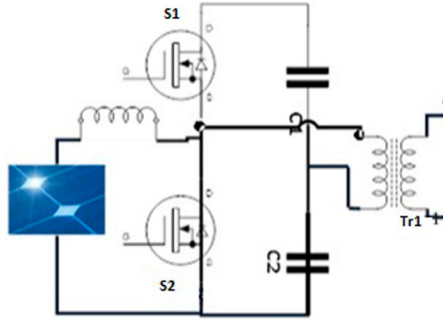


Figure 2. Hybrid boost resonant converter.

shown in Figures 2. In this circuit, two cascaded MOSFETs are integrated with the inductor in the middle leg. The overall design is kept simple by reducing the converter topology to two switches and an inductor in the middle with a constant frequency control.

The circuit tends to operate as a half-bridge resonant converter using the capacitors on the front and back ends of the transformer. The diodes on the secondary side maintain the circuit to be resonated perpetually. A single resonant period of a half-sine period is considered. The series resonance makes the circuit to turn ON and OFF by ZVS. Based on the dual switch operation, both the upper and the lower switches are triggered. This, in turn, operates the boost converter to reflect the changes on the output based on the duty ratio determined.

2.2. Functional operation of the front-end HBRC

The function of the hybrid boost resonant (HBRC) circuit is explained in different time stages. The voltage transfer ratio of the HBRC is given in (1), where n denotes the turns ratio of the step-up transformer and D_c is the duty cycle of the switch, S2.

$$\frac{V_0}{V_{in}} = \frac{\eta}{1 - D_c} \quad (1)$$

Stage 1 [$t_0 < t < t_1$]: The switch S2 is off. The current flows through the inductor and the diode of S1 settling its dependent capacitance. This turns ON S1 under zero voltage switching at t_0 . Resonance occurs through C1, leakage inductance of the transformer and capacitors C3 and C4 through D1. Simultaneously, input current starts charging C1 and C2. The mode 1 is over when D1 stops resonating and the current through the transformer reduces to zero. The duration of mode 1 is given by

$$T_{r1} = \pi \sqrt{L_2 \left[\frac{n^2(C_1 + C_2)(C_3 + C_4)}{C_1 + C_2 + n^2(C_3 + C_4)} \right]} \quad (2)$$

Stage 2 [$t_1 < t < t_2$]: S1 is active and it continues to conduct the input inductor current. The resonating

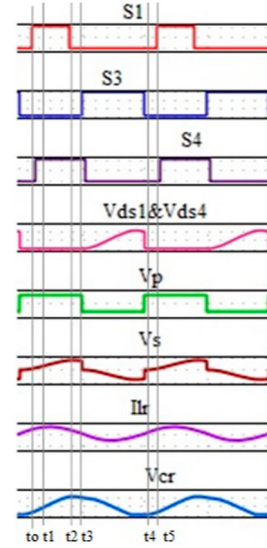


Figure 3. Waveforms of the resonant converter in the boost mode.

elements do not conduct current in this period, while C6 discharges through the load. Now, S1 turns OFF and S2 turns ON terminating mode 2.

Stage 3 [$t_2 < t < t_3$]: At this stage, the inductor current continues to charge C1 and C2 and it starts decreasing. Switching loss occurs due to the commutation of S1. Now the resonant current flows through C2, L2 and parallel combination of C3 and C4, through the diode D2. In this interval, the switch S2 carries the current of the transformer and the inductor. Mode 3 ends when the current through the transformer reduces to zero and its duration is given by

$$T_{r1} = \pi \sqrt{\frac{L_2 C_2 n^2 (C_3 + C_4)}{C_2 + n^2 (C_3 + C_4)}} \quad (3)$$

Stage 4 [$t_3 < t < t_4$]: The current through the inductor increases until the switch S2 is OFF and mode 1 resumes. The switch S1 prevents the charging or discharging of the upper capacitor during modes 3 and 4. The duration of mode 1 is more than mode 3 and it is based on the sizing of C1–C4 and the transformer turns ratio. The design involves the optimization of the duration of the resonant period. Figures 3 shows the waveforms of the HBRC.

2.3. Functional operation of the secondary controller

The output from the front-end boost conversion is given to the secondary controller which is used to obtain the DC step wave pattern based on the step level and the time. A modified voltage doubler with switches on the secondary side connects forms the

voltage regulation circuit. The secondary MOSFETs are triggered based on the voltage control with a phase regulation. Based on the voltage phase change, the voltage across the doubler can be altered, which, in turn, is used to generate the step-level voltage pattern. The four switches are operated in this cycle, as shown in Figures 4(a–d).

Stage 1 [t_0, t_1] [Figures 4(a)]: Before t_0 , the switches S2–S4 are in ON state, whereas the current is reset to zero. At t_0 , S2 is turned OFF. The inductor L1 behaves as a current source, thereby releasing the voltages of the switches S1 and S4. This results in the switching of S1 and S4 at zero voltage. Thus, the linear increase of current through the inductor L2 is given by

$$i_{L2}(t) = \frac{nV_{in}}{L_r}(t - t_0) \quad (4)$$

Stage 2 [t_1, t_2] [Figures 4(b)]: At t_1 , the switches S1, S3 and S4 turn ON with ZVS. The voltage of the circuit will rise towards V_{max} .

Stage 3 [t_2, t_3] [Figures 4(c)]: At t_2 , S1 and S4 turn OFF. The inductor L2 is charged and the converter acts as a series resonant converter. Now the resonance occurs through L2, C1 and C2.

Stage 4 [t_3, t_4] [Figures 4(d)]: At t_3 , S1 is ON and the capacitors C1 and C2 start charging again.

The current i_{Lr} and voltage v_{C1} are expressed as follows.

$$i_{L2}(t) = \frac{nV_{in}d\theta_s T_s}{L2} \quad (5)$$

$$i_{L2}(t) = \frac{r}{Z_r} \sin(\theta_1 + \omega_r(t - t_1)) \quad (6)$$

$$V_{C1}(t) = nV_{in} - r \cos(\theta_1 + \omega_r(t - t_1)) \quad (7)$$

where

$$r = \left| \frac{V_o}{2} - nV_{in} \right| + \Delta V_{C1} \quad (8)$$

$$\Delta V_{C1} = \frac{P_o T_s}{4V_o C3} \quad (9)$$

P_o is the output power and T_s is the switching period.

2.4. Maximum power point tracking

For any PV system, the output power can be increased by tracking the MPP (maximum power point) of the PV module by using a controller connected to DC–DC converter (usually boost converter). The proposed MPPT uses a fuzzy logic controller based on duty ratio variations. The photo voltaic system tracks the sunlight from the panel to give input for the resonant converter. But, unfortunately, the output of the PV system is a sinusoidal waveform which has a high

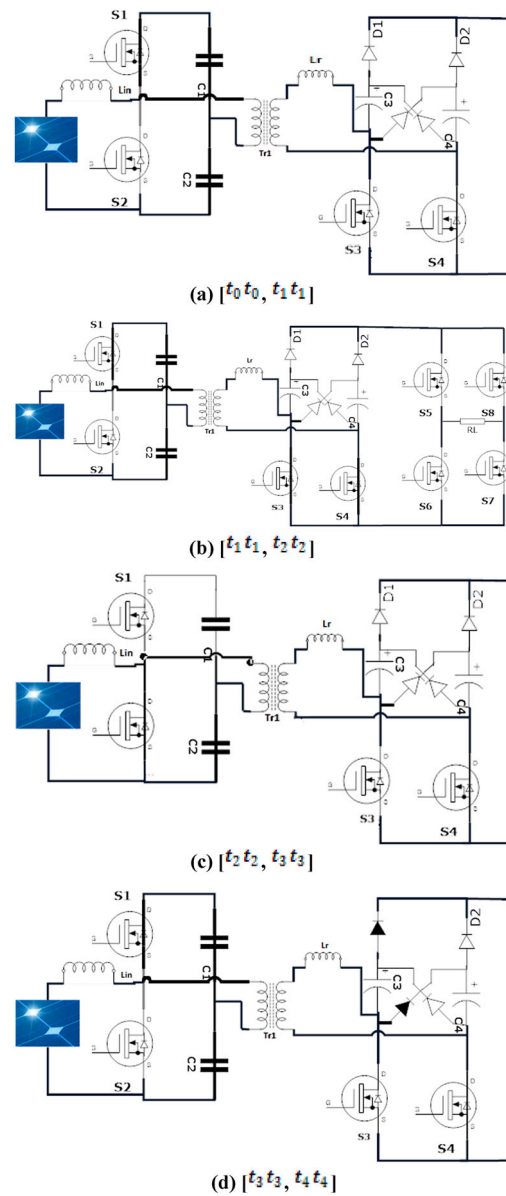


Figure 4. (a–d) Equivalent circuits in different stages; (a) [t_0, t_1]; (b) [t_1, t_2]; (c) [t_2, t_3] and (d) [t_3, t_4].

amount of harmonics. Its output is sent to the fuzzy-based MPPT controller that produces a non-sinusoidal step voltage waveform with reduced harmonics. When the voltage is triggered by the fuzzy controller, it delivers equal voltage to every step of the voltage waveform. The voltage varies at the regulator as per the voltage increase in the fuzzy controller. The phase shift controller is used to convert the output of the fuzzy controller into a sinusoidal waveform.

2.4.1. Proposed MPPT

The maximum power point tracking is implemented to ensure the maximum available peak power of the photovoltaic system to the load. In order to reach the peak power, the duty cycle of the converter is increased or decreased based on the voltage and current of the PV input. The HBRC is triggered alternatively to transfer the PV power to the transformer and to the load. By

turning on S2, the inductor charges the energy through the switch and releases when the switch is off. Alternatively, the S1 switch is turned ON to discharge the inductor energy to the capacitors C1 and C2 through the transformer. The duty ratio of the switches S1 and S2 determines the voltage gain ratio of the transformer. Altering the duty cycle of the converter alters both the input and the output voltage as well as the current. The duty ratio can be defined as

$$D = \frac{t_{\text{on}}}{t_{\text{on}} + t_{\text{off}}} = \frac{t_{\text{on}}}{T_d} \quad (10)$$

where switch on $t_{\text{on}} : \Delta I_L^+ = (V_i/L)t_{\text{on}}$

switch off $t_{\text{off}} : \Delta I_L^- = (V_i - V_o/L)t_{\text{off}}$

Generally, perturb and observe [P&O] techniques are widely deployed maximum power tracking schemes for various PV systems. These methods follow a periodical perturbation which tends to change the duty cycle over a period of time which will result in an oscillation at the maximum power point, i.e. due to the perturbation cycle, the change of the peak power cannot be exactly determined in the peak power point, the cycle would determine peak power and tries to operate to the peak point; in this case, the change of the voltage and current would be found on the input and the output of the converter; as a result, the next perturbation would oscillate as the input voltage or current would start to decrease which results in peak power oscillation, which, in turn, results in power loss. In order to minimize the peak power oscillations, the incremental conductance methods are used. The INC operation is based on the previous operating point. This reduces the peak oscillations but tends to reduce the duty ratio speed to reach the maximum operating point due to the change of the duty cycle. In order to enhance the speed of the maximum power point operation, a variable-step incremental conductance is implemented.

$$\frac{dP}{dV} = 0 \quad (11)$$

$$\frac{dI}{dV} \approx -\frac{I - I_o}{V - V_o} = -\frac{\Delta I}{\Delta V} \quad (12)$$

2.4.2. Fractional INC

The change of the voltage V_o is used to determine the step size of the MPP tracker. In order to change the step size, the voltage, power and current are taken as the inputs and the slopes of the variables are taken as the reference. Fractional order of the slopes is used to determine the required step for the duty ratio change. Figures 5 shows the flowchart of fractional INC.

The fractional-order differentiator is applied as non-linear feedback control where the generalized fractional order is expressed as

$$D_t^\alpha t^n = \frac{\partial(m+1)}{\partial(m+1-\varphi)t^{m-\varphi}} \quad (13)$$

where ∂ represents the function and φ represents the derivative and its value bounds under $0 < \varphi < 1$. Implementing the fractional order to the incremental conductance can be rewritten as

$$\frac{d^\alpha I}{dV^\alpha} \approx \lim_{\Delta V \rightarrow 0} \frac{I(V) - \alpha I(V - \Delta V)}{\Delta V^\alpha} \quad (14)$$

$$\frac{d^\alpha I}{dV^\alpha} \approx \frac{I - \alpha I_o}{(V - V_o)^\alpha} \quad (15)$$

When $\alpha = 1$, the slope lies in the straight line, hence $0 < \alpha < 1$ forms the fractional-order derivative which can be rewritten as

$$\frac{d^\alpha}{dV^\alpha} \left(-\frac{I_o}{V_o} \right) = \left(-\frac{1}{V_o} \right) \frac{d^\alpha I_o}{dV^\alpha} + (-I_o) \frac{d^\alpha V_o^{-1}}{\Delta V^\alpha} \quad (16)$$

$$= \left(-\frac{1}{V_o} \right) \frac{\gamma(2)}{\gamma(2-\alpha)} (I_o)^{1-\alpha} + (I_o) \frac{\gamma(0)}{\gamma(-\alpha)} V_o^{-1-\alpha} \quad (17)$$

The MPP approximation is done through the variable derivative value α which lies with the slope of change of power to the differential power which lies on the curve of $\alpha = 1$ of the fractional order that makes the steady-state error that has a large response over the steady-state MPP tracking compared to perturbation scheme.

The change of the voltage, current $\Delta v = (V - V_o)$, $\Delta I = (I - I_o)$ and the slope $\Delta p/\Delta v$ of the power-voltage curve are calculated as the variance. The variation of the voltage and current with the fractional-order differentiator can be expressed as $d^\alpha I = I - \alpha I_o$ and the voltage can be defined as $dV^\alpha = V - \alpha V_o$ where α is the derivative number and initially considered as 1 and decremented as the change of variance.

3. Generation of multilevel pattern

3.1. Generation of the multilevel PWM pattern using phase shift controller

The output voltage V_{out} of the secondary converter consists of two modes, namely boost mode and buck mode. The boost mode is the mode having a step voltage higher than the maximum voltage, whereas buck mode constitutes with the lower step voltage. In order to obtain variable voltage levels, phase shift PWM is applied to the dual switches of the secondary side controller. The reference signal V_{max} and V_{min} are fixed, whereas V_{step} varies with n -step. The main use of the phase shift controller is to optimize the step voltage V_{step} which is given by

$$V_{\text{step}} = \frac{V_{\text{max}}}{n_{\text{step}}} \quad (18)$$

The reference signal V_{max} is defined by the number of levels and the frequency. The time period of the step

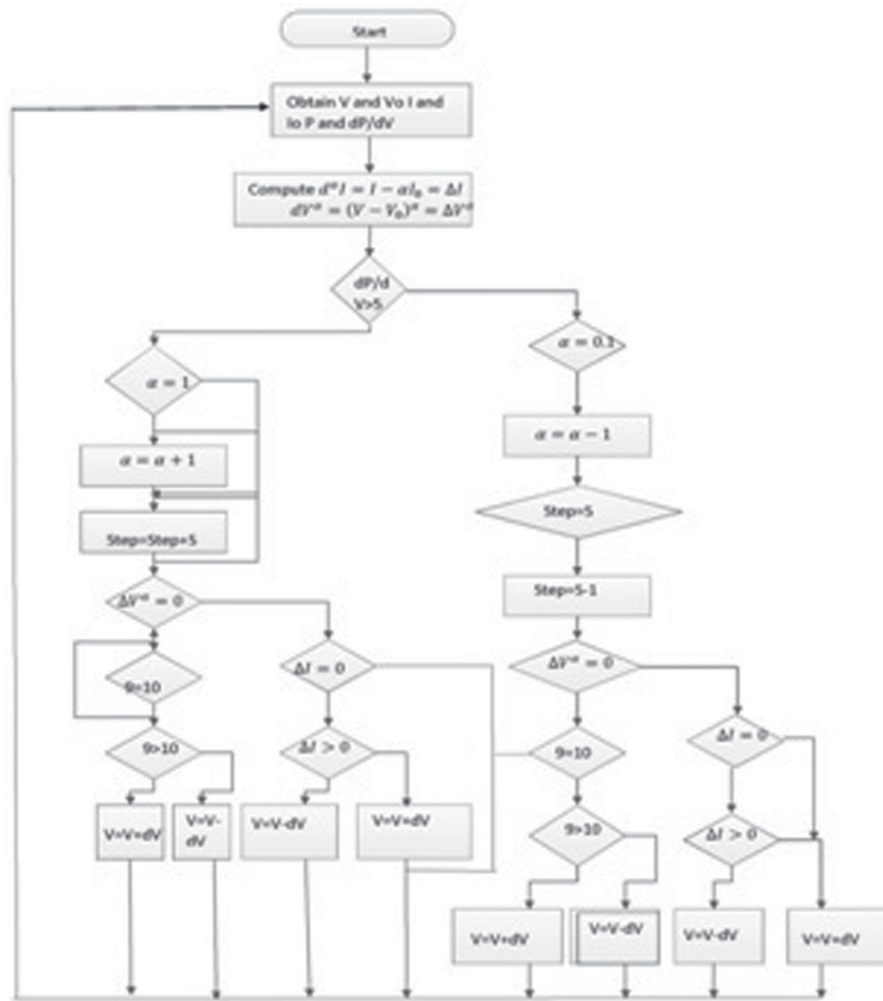


Figure 5. Flowchart of the fractional INC.

waveform of half cycle is calculated as

$$t_{1/2} = \frac{1}{2f} \quad (19)$$

In the step waveform, the half cycle (increment mode) works with the boost mode and the other half cycle (decrement mode) works with the buck mode. The time period for the every step of the waveform is given by

$$T_{\text{step}} = \frac{t_{1/2}}{n_{\text{step}}} \quad (20)$$

In the case of the step waveform, the voltage should be equally distributed in every step with respect to time. When DC voltage is applied, only 90% of the voltage is given. To gain the full output, fuzzy is added which improves the full voltage. The voltage at the fuzzy controller is set as V_{set} which is given by

$$V_{\text{set}} = \frac{\Delta V}{\Delta T_{\text{step}}} \quad (21)$$

When the DC voltage is given at the switch S4 which is open, it delivers the output and then fuzzy is implemented to draw the remaining duty cycle from where

it stops. Thus, the process repeats for $n/2$ step of the waveform and it is achieved within the respective time period. After the incremental step is attained completely, the controller is switched to the buck mode which starts to reduce the voltage. When the switch S4 is closed, the voltage drops and it is controlled by the duty cycle control. The process is performed as mentioned in the following steps.

Step 1: Consider 350 V is fed as input for 10-level step waveform. Now, the voltage for a single step is 70 V at the incremental mode.

Step 2: The time taken for the full cycle of step waveform is 20 ms. Hence, 10 ms is required for half cycle which has 10 steps. Therefore, it is clear that 1 ms is needed by every step for the duty cycle control.

Step 3: When V_{max} is applied, the switch S4 is opened. It starts with the boost mode where the duty cycle is varied up to 63 V and the remaining 10% of the duty cycle control is done by the fuzzy. The voltage is given as $V_{\text{set}} = 10\%$ of $(\Delta V / \Delta T_{\text{step}})$.

Step 4: After the step achieves the optimum level, the control is given to start the next duty cycle after a certain interval.

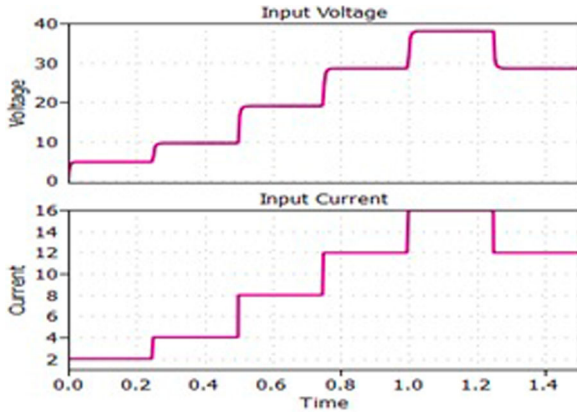


Figure 6. Voltage and current with respect to solar irradiance.

Step 5: The above-mentioned steps are repeated for five steps of the step waveform and until it reaches V_{\max} and the controller shifts to the buck mode for the reverse process.

Step 6: In the buck mode, the switch S4 is closed, the voltage drops gradually within the time period of 1 ms and controlled for the next duty cycle process. The process is repeated for five steps of the step waveform. Thus, 350 V is distributed in 10 steps for the half cycle which is repeated for the negative half cycle. The full cycle with applied voltage 350 V for the time of 10 ms is executed as described.

This results in an array of reference levels equally distributed with respect to time for every step change. The sinusoidal signal is compared with the step-change array to modify the duty ratio. The duty cycle (D_c) is the ratio of the duration of a single pulse width (T_p) and the total time period of the step waveform (T_{step}).

$$D_c = \frac{T_p}{T_{\text{step}}} \quad (22)$$

When a single step of the duty cycle is finished, the duty cycle of the next step of the waveform has to be initiated with the result of the preceding result. The delay of the duty cycle should be limited and the net value of the n -step duty cycle is given by

$$\Delta D_c = \frac{D_{c(\max)}}{n} + \Delta D_{\min} \quad (23)$$

where ΔD_{\min} the duty cycle of the previous step and $D_{c(\max)}$ is given by

$$D_{c(\max)} = \frac{V_{\max}}{V_{\text{in}}} \quad (24)$$

The output of the fuzzy controller is phase shifted by comparing the sine waveform of V_{in} with two triangular waveforms that are 180° shifted from each other.

3.2. Level unfolding

The output of the converter is fed to the H-bridge inverter which has four switches (S5, S6, S7 and S8

as shown in Figures 1). The H-bridge inverter is used to convert m -level DC voltage (V_b) obtained from the HBRC converter into n -level AC output voltage (V_o). When S5 and S8 are switched ON, by the gate pulse, the positive output voltage is obtained at the load ($V_o = +V_b$). When S5 and S8 are switched ON and when S6 and S7 are switched ON, the output voltage obtained at the load is zero ($V_o = 0$). When S6 and S7 are switched ON, the negative output voltage is obtained at the load ($V_o = -V_b$). Thus, the inverter generates multilevel AC voltage, as required.

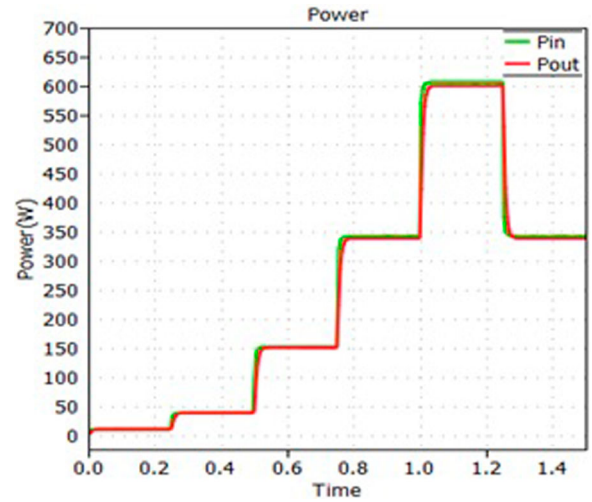
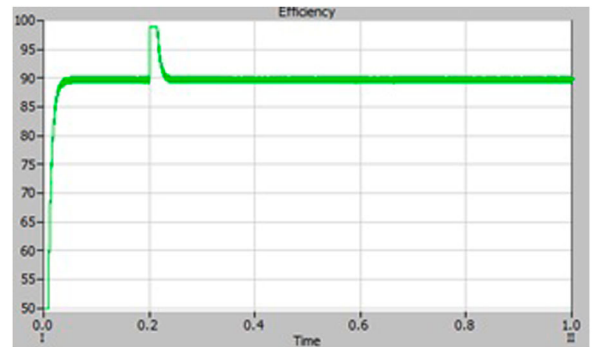
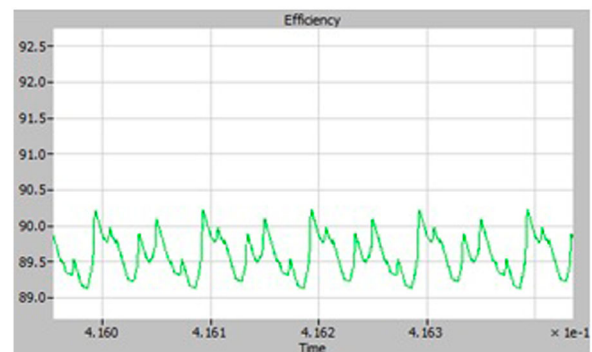


Figure 7. Efficacy of the converter.



(a)



(b)

Figure 8. (a) Step-change variation of P&O and (b) Peak oscillation of P&O.

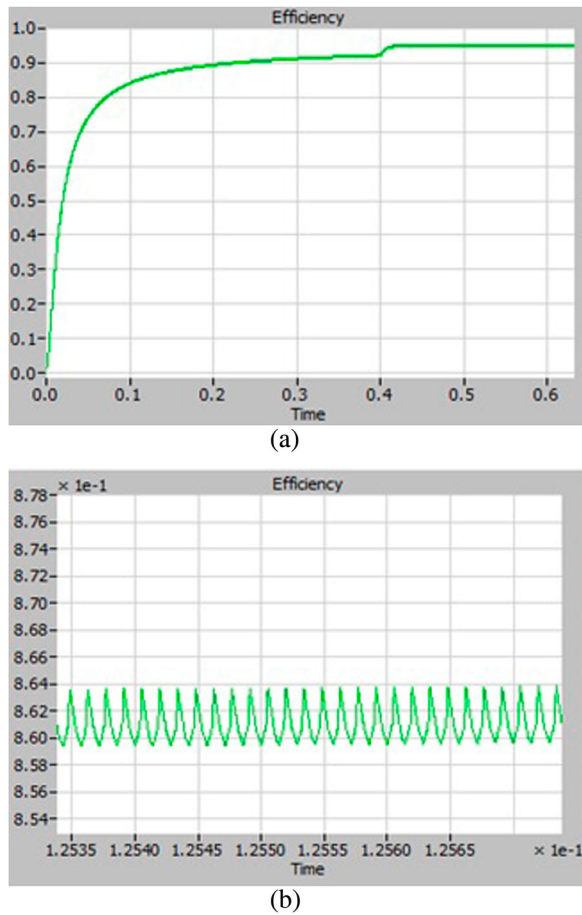


Figure 9. (a) Step-change variation of the proposed MPPT and (b) peak oscillation of the proposed MPPT.

4. Experimental section

To illustrate the performance of the proposed work, its model has been simulated and results were obtained. The same is implemented with the hardware prototype with a solar input which is kept around 40–60 V, the switching frequency f_s is 15 kHz and the fundamental frequency f is 50 Hz. The front-end converter operates

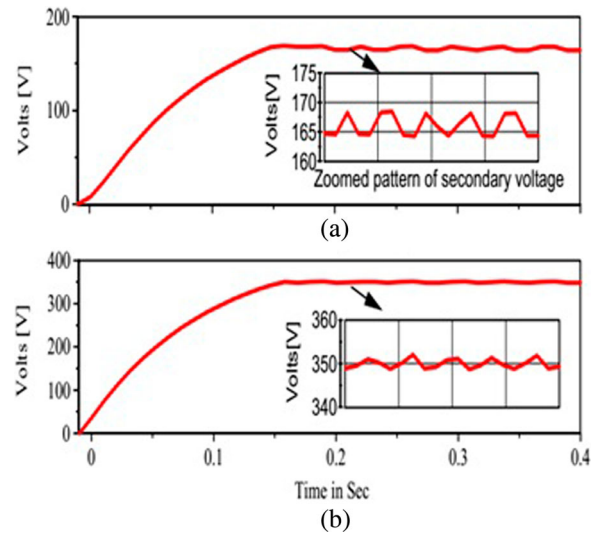


Figure 10. (a) Regulated voltage output at the secondary side of the transformer and (b) voltage doubler output.

around the DC voltage of 40–60 V which is further boosted and stepped the secondary to transform as an AC-stepped voltage pattern. The MOSFETs chosen are IRF540N for the front end and IRF840N for the back end. The value of the inductor chosen is 680 mH, while the capacitors C1 and C2 are kept as 47 μ F and C3 and C4 to be 100 μ F. The front-end converter is made to operate under the peak power of the PV panel through fractional-order maximum power point tracker. The secondary side step control is regulated through the fuzzy controller followed by a phase shift controller.

Figures 6 shows the power change of the system with a step change of the solar irradiance and the change of the voltage and the current.

Figures 7 shows the convergence efficacy of the converter, in which the power tracking is obtained with a minimal time without a larger variation of the duty cycle that leads to power oscillations. The step change of input power is tracked with a differential order tracker.

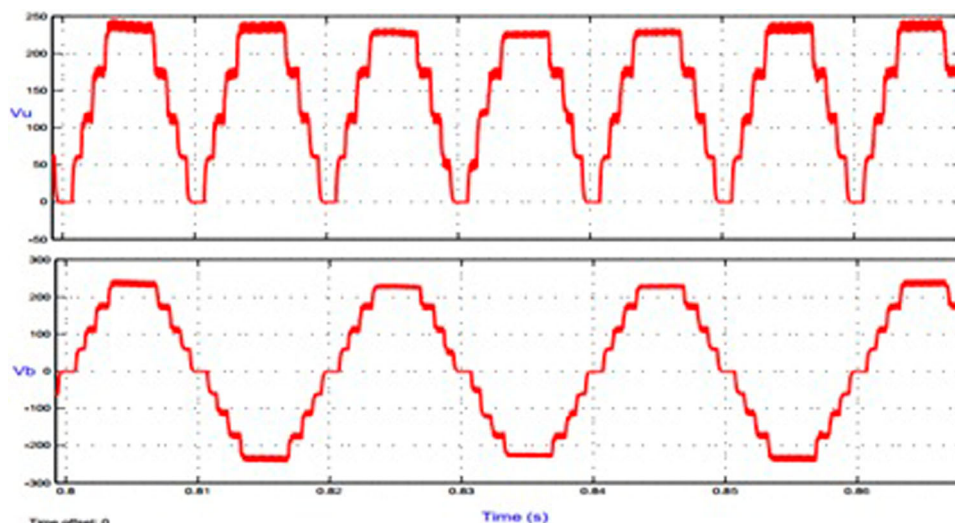


Figure 11. m-level unipolar output from the converter and n-level bipolar output from the inverter.



Figure 12. PWM wave of the converter; unipolar output from the converter; load current variation.

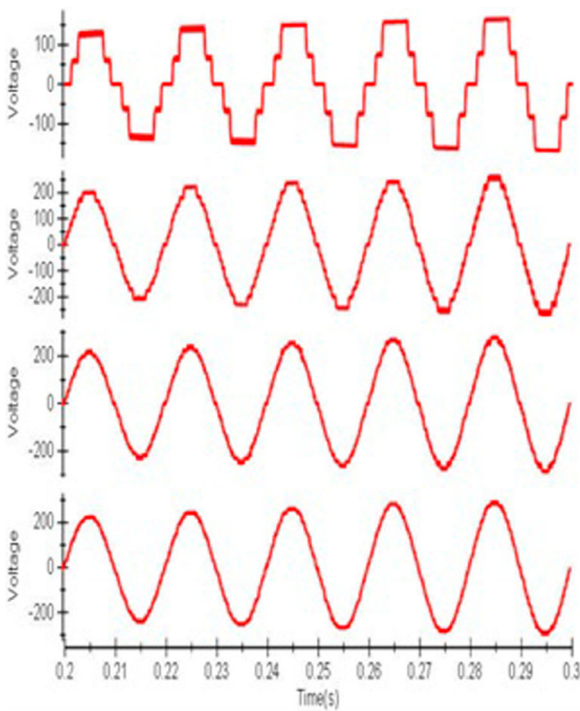


Figure 13. Waveform of output AC voltage of the proposed configuration for various levels: (a) 5 levels, (b) 15 levels, (c) 25 levels, (d) 49 levels.

The step-change variation and peak oscillation of the P&O technique and the proposed MPPT are shown in Figures 8 and 9.

The DC voltage V_{in} obtained from the PV panel is applied to the front converter. Since the output voltage of the PV array is variable depending on the solar irradiation, the front-end converter is operated on the PV panel peak power by varying the duty ratio. In order to reach the peak power over a period of voltage, the power inputs are perturbed. Based on the fractional power change corresponding to the voltage, the duty cycle is determined and applied to the half-bridge legs of the front-end converter with inverted to each other. The voltage obtained from the converter is switched to

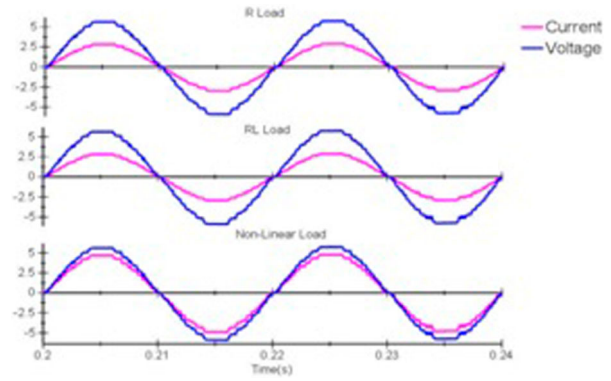
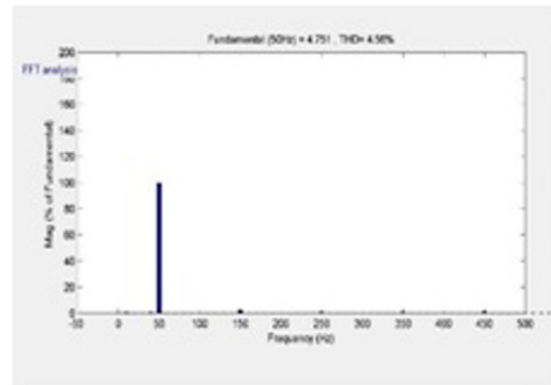
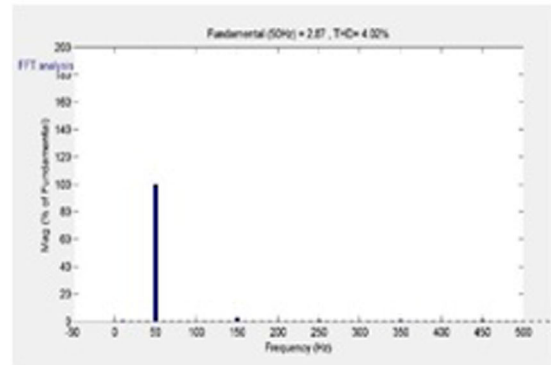


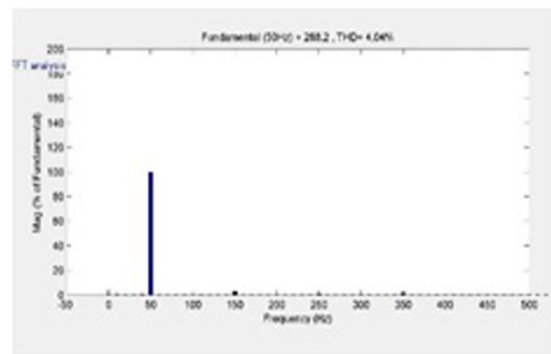
Figure 14. Voltage–current ($V-I$) waveform of the proposed topology with R-load, RL-load and non-linear load.



(a)



(b)



(c)

Figure 15. (a) THD of non-linear load, (b) THD of RL-load, (c) THD of R-load for 25-level output voltage.

the transformer secondary which steps up for a high-voltage DC and is further split to various voltage levels programmatically.

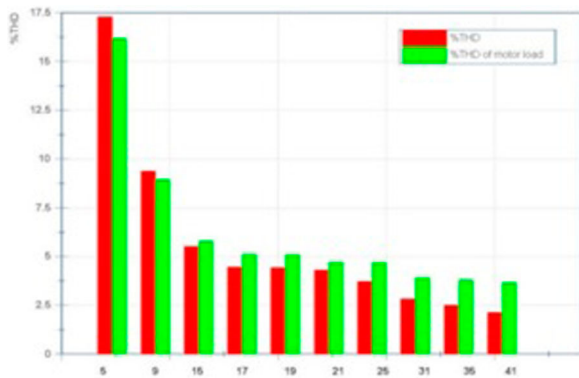


Figure 16. % THD of converter output for a variety of levels.

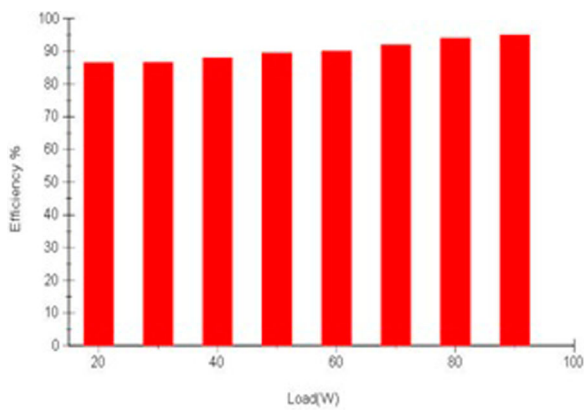


Figure 17. Load vs efficiency.

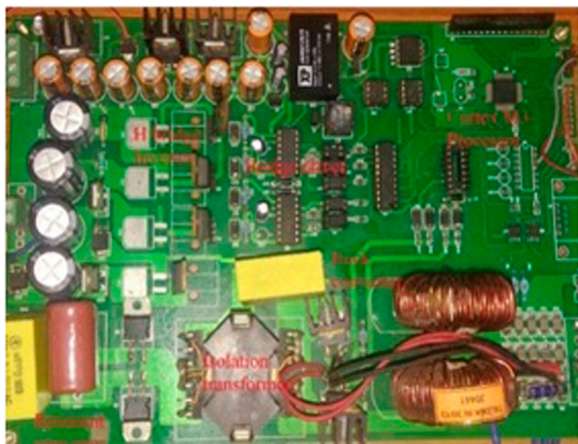


Figure 18. Hardware set-up of the proposed topology.

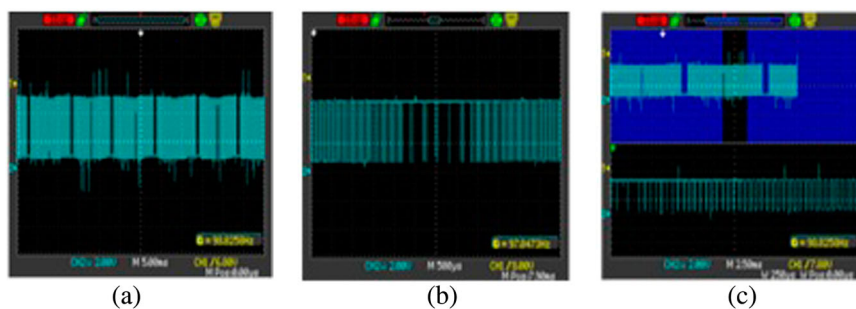


Figure 19. (a) PWM pattern of the inverter (b) zoomed view of the PWM pattern (c) PWM and zoomed view waveform of the inverter.

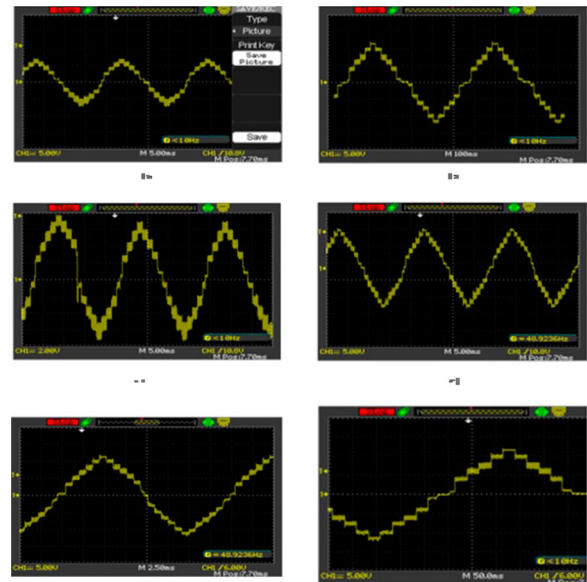


Figure 20. Scope waveform for the inverter output voltage for various levels. (e) and (f) represent the zoomed view of the inverter output voltage.

The DC-regulated stepped voltage without the inverter-connected condition is shown in Figures 10(a). The transformer steps up the voltage up to a certain level due to the concern of the size and losses. Hence, the voltage is boosted to the required value by varying the secondary switches at the doubler circuit. The voltage output of the doubler circuit is shown in Figures 10(b). This circuit also rectifies and regulates the DC output. Figures 10(b) shows the desired high DC output voltage.

The waveforms of the secondary DC voltage to the inverter and the multilevel-transformed unipolar output from the converter and m -level bipolar output from the inverter are shown in Figures 11.

Figures 12 shows the different duty cycle PWM pulses to each step of the output. The variation of duty ratio is shown in the figure for different levels. The duty ratio is less for the first-level voltage, then it increases for the second-level voltage and so on. Initially for 90% of V_{step} , the duty cycle of each step voltage is D_{max} and after that, it is taken over by the FLC-based phase shift modulation. Figures 13 shows the waveform of the output AC voltage of the proposed configuration for various levels.

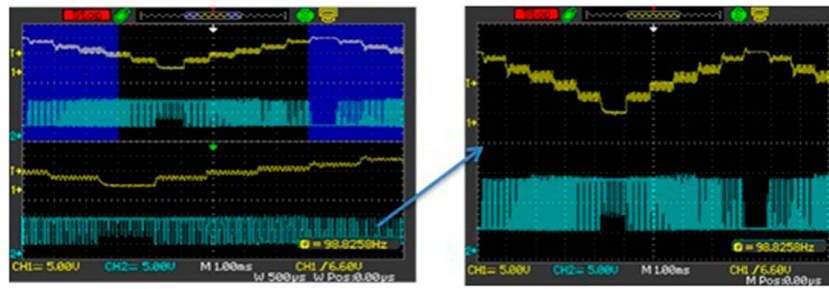


Figure 21. Inverter output for the corresponding PWM.

Figures 14 shows the voltage and current waveforms obtained at the output side for different types of loads such as R-load, RL-load and non-linear load with a voltage pattern downscaled for representing the current and the voltage under a phase.

The voltage and current waveforms for various loads obtained at 230 V are scaled down to 5 V for a clear view as shown in Figures 14.

Figures 15 depicts the total harmonic distortion (THD) of the proposed configuration for output voltage with 25 levels for three different cases. The response of the inverter for various load combinations exhibits lower harmonic contents. As the inverter levels go down, the harmonic contents may change. It is observed that the THD reduces with a variety of levels. As the proposed inverter is capable of producing multiple levels in the output voltage, by increasing the number of levels THD can be significantly reduced as shown in Figures 16.

The THD percentage comparison for a variety of levels with R-load is shown in Figures 16.

From the figure, it can be clearly seen that, as the levels increase, the harmonic content reduces. The above inverter configuration is validated up to a maximum of 41 levels, which poses higher harmonic contents at the lower levels and then the harmonics decrease with an increase in the step levels. The harmonic levels are drastically reduced at higher levels of the voltage step. The variation of efficiency for different load levels is shown in Figures 17.

The hardware set-up of the proposed method is shown in Figures 18. Figures 19–21 show the PWM and converter output waveforms in the scope with multiple levels.

5. Conclusion

The proposed multilevel inverter, which generates voltage step levels as programmed based on the hybrid boost resonant converter as the front-end converter with an MPPT control based on fractional INC, and a back-end phase shift controller-based pattern generation with an H-bridge inverter, is designed and validated with a prototype. The proposed inverter that is validated against larger PV variations provides a good

tracking pattern with better efficiency and voltage control. The secondary side phase shift regulation is used to generate the desired number of levels in the output voltage. The multilevel inverter end is regulated with a suitable pulse width based on the fuzzy control. The step generation, initiated with constant duty with a maximum limit and regulated to the reference voltage step with the fuzzy control, has been verified. The multilevel inverter can be programmed to generate voltage up to n level. The MOSFETs of the secondary side are turned ON and OFF by the phase shift modulation, while the primary side is regulated to PV power with fractional INC. The multilevel and the PV power variations are obtained as expected. The secondary control is regulated based on the single-step control, in which each step voltage is controlled partly by DC input voltage with a constant D_{max} and fuzzy-based phase shift modulation in the ratio 9:1 that provides a full step voltage and equal voltage distribution over the cycle. It can be observed from the front-end converter control that the fractional INC produces less peak oscillations at the MPP compared to the traditional peak power trackers. Moreover, the input voltage variation during the step change of the PV power is regulated at the secondary side to obtain the step levels with equally distributed voltage. It can be observed that increased step levels display lower-level harmonic contents. From the results, it is observed that the waveform for less number of step levels contains lower-level DC ripples due to slower variations of the potentials, while it is absent with larger levels that makes the converter suitable for varying output levels of various power applications.

Disclosure statement

No potential conflict of interest was reported by the authors.

References

- [1] Li CW, He X. Review of non-isolated high step-up DC/DC converters in photovoltaic grid-connected applications. *IEEE Trans Ind Electron.* 2011;58(4): 1239–1250.
- [2] Zhao Q, Lee FC. High-efficiency, high step-up DC–DC converters. *IEEE Trans Power Electron.* 2003;18(1): 65–73.

- [3] Wai R-J, Duan R-Y. High step-up converter with coupled-inductor. *IEEE Trans Power Electron.* 2005; 20(5):1025–1035.
- [4] Wai RJ, Duan RY. High-efficiency power conversion for low power fuel cell generation system. *IEEE Trans Power Electron.* 2005;20(4):847–856.
- [5] Gules R, et al. A modified SEPIC converter with high static gain for renewable applications. *IEEE Trans Power Electron.* 2014;29(11):5860–5871.
- [6] Lopez O, Teodorescu R, Freijedo F, et al. Leakage current evaluation of a single-phase transformerless PV inverter connected to the grid; United states: Applied power Electronics Conference, APEC; 2007.
- [7] Yu W, Lai J-S, Qian H, et al. High-efficiency MOSFET inverter with H6-type configuration for photovoltaic non-isolated ac module applications. *IEEE Trans Power Electron* 2011;26:1253–1260.
- [8] Kerekes T, Teodorescu R, Borup U. Transformerless photovoltaic inverters connected to the grid; 25.02.2007; Anaheim, United States: Applied Power Electronics Conference, APEC; 2007.
- [9] Liang T-J, et al. Novel isolated high-step-up DC-DC converter with voltage lift. *IEEE Trans Ind Electron.* 2013;60(4):1483–1491.
- [10] Martins DC, Demonti R. Photovoltaic energy processing for utility connected system. *Industrial Electronics Society, IECON; 2001.* p. 1292–1296, vol. 2.
- [11] Roman E, Alonso R, Ibanez P, et al. Intelligent PV module for grid-connected PV systems. *IEEE Trans Ind Electron* 2006;53:1066–1073.
- [12] Hsieh Y-C, Chen M-R, Cheng H-L. An interleaved flyback converter featured with zero-voltage transition. *IEEE Trans Power Electron* 2011;26:79–84.
- [13] Spiazzi G, Mattavelli P, Costabeber A. High step-up ratio flyback converter with active clamp and voltage multiplier. *IEEE Trans Power Electron* 2011;26: 3205–3214.
- [14] Gu Y, Hang L, Lu Z, et al. Voltage doubler application in isolated resonant converters; 6-10 Nov. 2005; Raleigh, NC, USA: Industrial Electronics Society, IECON; 2005.
- [15] Lu B, Liu W, Liang Y, et al. Optimal design methodology for LLC resonant converter; 19-23 March 2006; Dallas, TX, USA: Applied Power Electronics Conference, APEC; 2006.
- [16] Lazar JF, Martinelli R. Steady-state analysis of the LLC series resonant converter; 4-8 March 2001; Anaheim, CA, USA: Applied Power Electronics Conference, APEC; 2001. vol. 2.
- [17] York B, Yu W, Lai J-S. An integrated boost resonant converter for photovoltaic applications. *IEEE Trans Power Electron.* 2013;28(3):1199–1207.
- [18] Hwang C, Leu J-F, Tsay S-Y. A note on time-domain simulation of feedback fractional-order systems. *IEEE Trans Automat Contr.* 2002;47(4):625–631.
- [19] Lin C-H, Huang C-H, Du Y-C, et al. Maximum photovoltaic power tracking for the PV array using the fractional-order incremental conductance method. *Appl Energy.* 2011;88(12):4840–4847.
- [20] Hussein KH, Muta I, Hoshino T, et al. Maximum photovoltaic power tracking: an algorithm for rapidly changing atmospheric conditions. *IEEE Proceedings: Generation, Transmission and Distribution.* 1995; 142(1):59–64.
- [21] Kwon J-M, Nam K-H, Kwon B-H. Photovoltaic power conditioning system with line connection. *IEEE Trans Ind Electron.* 2006;53(4):1048–1054.
- [22] Zhou X, Song D, Ma Y, et al. The simulation and design for MPPT of PV system based on incremental conductance method. *Proceedings of the WASE International Conference on Information Engineering (ICIE '10).* Hebei, China; 2010. p. 314–317.